AIAA 94-0572

Observations of Methane and Ethylene Diffusion Flames Stabilized Around a Blowing Porous Sphere under Microgravity Conditions

A. Atreya and S. Agrawal
Department of Mechanical Engineering
and Applied Mechanics
The University of Michigan
Ann Arbor, MI 48109-2125

K. R. Sacksteder
Microgravity Combustion Research
NASA Lewis Research Center
Cleveland, OH 44135

H. R. Baum
National Institute of Standards and Technology
Gaithersburg, MD 20899

32nd Aerospace Sciences Meeting & Exhibit
January 10-13, 1994 / Reno, NV

OBSERVATIONS OF METHANE AND ETHYLENE DIFFUSION FLAMES STABILIZED AROUND A BLOWING POROUS SPHERE UNDER MICROGRAVITY CONDITIONS

Arvind Atreya and Sanjay Agrawal
Combustion and Heat Transfer Laboratory
Department of Mechanical Engineering and Applied Mechanics
The University of Michigan, Ann Arbor, MI 48109-2125

Kurt R. Sacksteder
Microgravity Combustion Research
NASA Lewis Research Center
Cleveland, OH 44135

Howard R. Baum
National Institute of Standards and Technology
Gaithersburg, MD 20899

Abstract

This paper presents the experimental and theoretical results for expanding methane and ethylene diffusion flames in microgravity. A small porous sphere made from a low-density and low-heat-capacity insulating material was used to uniformly supply fuel at a constant rate to the expanding diffusion flame. A theoretical model which includes soot and gas radiation is formulated but only the problem pertaining to the transient expansion of the flame is solved by assuming constant pressure infinitely fast one-step ideal gas reaction and unity Lewis number. This is a first step toward quantifying the effect of soot and gas radiation on these flames. The theoretically calculated expansion rate is in good agreement with the experimental results. Both experimental and theoretical results show that as the flame radius increases, the flame expansion process becomes diffusion controlled and the flame radius grows as $\sqrt{t}$. Theoretical calculations also show that for a constant fuel mass injection rate a quasi-steady state is developed in the region surrounded by the flame and the mass flow rate at any location inside this region equals the mass injection rate.

I. Introduction

The absence of buoyancy-induced flows in a microgravity environment and the resulting increase in the reactant residence time significantly alters the fundamentals of many combustion processes. Substantial differences between normal gravity and microgravity flames have been reported during droplet combustion[1], flame spread over solids[2,3], candle flames[4] and others. These differences are more basic than just in the visible flame shape. Longer residence time and higher concentration of combustion products create a thermochemical environment which changes the flame chemistry. Processes such as soot formation and oxidation and ensuing flame radiation, which are often ignored under normal gravity, become very important and sometimes controlling. As an example, consider the droplet burning problem. The visible flame shape is spherical under microgravity versus a teardrop shape under normal gravity. Since most models of droplet combustion utilize spherical symmetry, excellent agreement with experiments is anticipated. However, microgravity experiments show that a soot shell is formed between the flame and the evaporating droplet of a sooty fuel[1]. This soot shell alters the heat and mass transfer between the droplet and its flame resulting in significant changes in the burning rate and the propensity for flame extinction. This change in the nature of the process seems to have occurred because of two reasons: (i) The soot formed could not be swept out of the flame due to the absence of buoyant flows. Instead, it was forced to go through the high temperature reaction zone increasing the radiative heat losses, and (ii) soot formation was enhanced due to an increase in the reactant residence time.

Recently, some very interesting observations of candle flames under various atmospheres in microgravity have been reported[4]. It was found that for the same atmosphere, the burning rate per unit wick surface area and the flame temperature were considerably reduced in microgravity as compared with normal gravity. Also, the flame (spherical in microgravity) was much thicker and further removed from the wick. It thus appears that the flame becomes "weaker" in microgravity due to the absence of buoyancy generated flow which serves to

transport the oxidizer to the combustion zone and remove the hot combustion products from it. The buoyant flow, which may be characterized by the strain rate, assists the diffusion process to execute these essential functions for the survival of the flame. Thus, the diffusion flame is "weak" at very low strain rates and as the strain rate increases the flame is initially "strengthened" and eventually it may be "blown-out." The computed flammability boundaries[5] show that such a reversal in material flammability occurs at strain rates around 5 sec^{-1}. Model calculations for a zero strain rate *1-D* diffusion flame show that even gas radiation is sufficient to extinguish the flame[6].

The above observations suggest that flame radiation will substantially influence diffusion flames under microgravity conditions, particularly the conditions at extinction. This is because, flame radiation at very low or zero strain rates is enhanced due to: (i) high concentration of combustion products in the flame zone which increases the gas radiation, and (ii) low strain rates provide sufficient residence time for substantial amounts of soot to form which is usually responsible for most of the radiative heat loss. It is anticipated that this radiative heat loss may extinguish the already "weak" diffusion flame.

To investigate the possibility of radiation-induced extinction limits under microgravity conditions, spherical geometry is chosen. This is convenient for both experiments and theoretical modeling. In this work, a porous spherical burner is used to produce spherical diffusion flames in μg. Experiments conducted with this burner on methane (less sooty) and ethylene (sooty) diffusion flames are described in the next section. A general theoretical model for transient radiative diffusion flames is then formulated and calculations are presented for the transient expansion of the spherical diffusion flame. These calculations are compared with the experimental measurements in the discussion section. This work is the first necessary step toward investigating radiative-extinction of spherical diffusion flames.

II. Experimental Apparatus and Results

The μg experiments were conducted in the 2.2 sec drop tower at the NASA Lewis Research Center. The experimental drop-rig used is schematically shown in Color Plate 1. It consists of a test chamber, burner, igniter, gas cylinder, solenoid valve, camera, computer and batteries to power the computer and the solenoid valves. The spherical burner (1.9 cm in diameter) is constructed from a low density and low heat capacity porous ceramic material. A 150 cc gas cylinder at approximately 46.5 psig is used to supply the fuel to the porous spherical burner. Typical gas flow rates used were in the range of 3-15 cm^3/s. Flow rates to the burner are controlled by a needle valve and a gas solenoid valve is used to open and close the gas line to the burner upon computer command. An igniter is used to establish a diffusion flame. After ignition the igniter is quickly retracted from the burner and secured in a catching mechanism by a computer-controlled rotary solenoid. This was necessary for two reasons (i) The igniter provides a heat sink and will quench the flame (ii) Upon impact with the ground (after 2.2 sec) the vibrating igniter may damage the porous burner.

As shown in the Color Plate 1, the test chamber has a 5" diameter Lexan window which enables the camera to photograph the spherical diffusion flame. The flame growth can be recorded either by a 16mm color movie camera or by a color CCD camera which is connected to a video recorder by a fiber-optic cable during the drop. Since the fuel flow may change with time, it had to be calibrated for various settings of the needle valve for both methane and ethylene. A soap bubble flow meter was used to calibrate the flow for various constant gas cylinder pressures. Constant pressures were obtained by connecting the cylinder to the main 200 lb gas cylinder using a quick-disconnect. An in-line pressure transducer was used to obtain the transient flow rates. Changes in the cylinder pressure during the experiment along with the pressure-flow rate calibration, provides the transient volumetric flow rates. These are shown plotted in Figure 1.

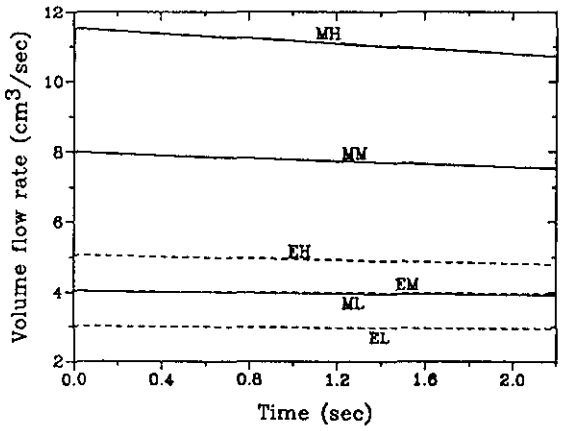

Figure 1: Volume flow rates versus time.

In Figure 1, the letters "M" and "E" represent methane and ethylene respectively and the letters "L", "M" and "H" represent low, medium and high flow rates. Thus, MM implies medium flow rate of methane. Note that low flow rate for methane is nearly equal to the medium flow rate of ethylene. For these experiments, the gas velocity at the burner wall was 0.25-1 cm/sec.

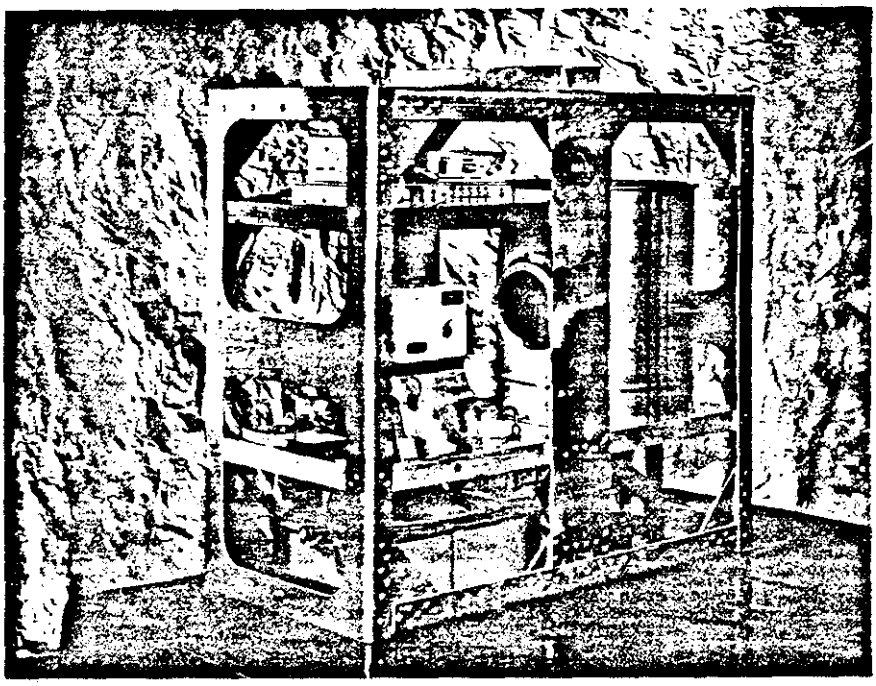

Picture of the microgravity spherical diffusion flame apparatus

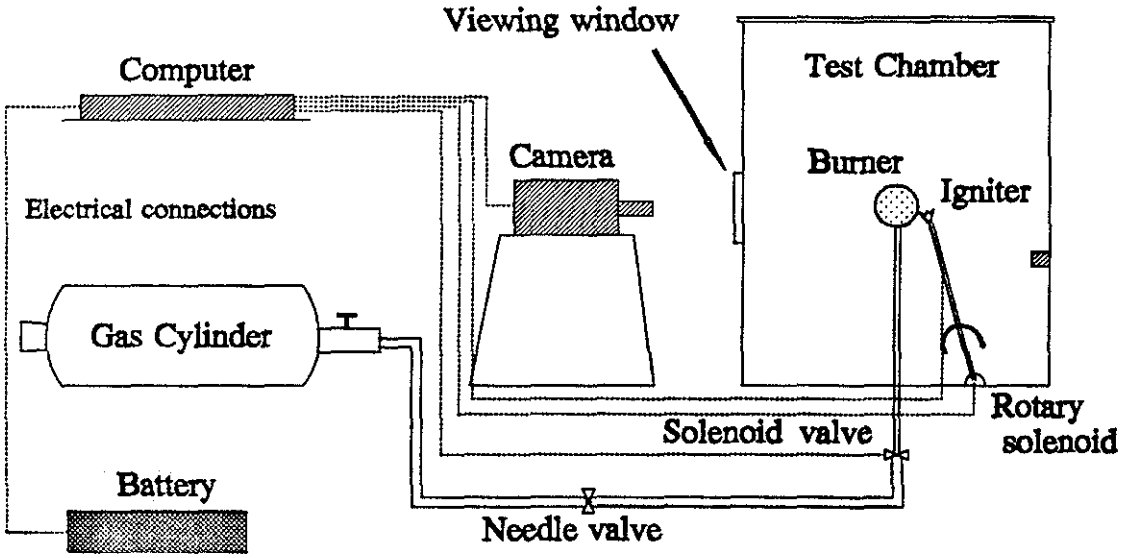

Schematic of the microgravity spherical diffusion flame apparatus

COLOR PLATE 1

The porous spherical burner produced a nearly spherical diffusion flame in microgravity. Some observed disturbances are attributed to slow large-scale air motion inside the test chamber. Several microgravity experiments were performed under ambient pressure and oxygen concentration conditions for different flow rates of methane and ethylene (as shown in Fig. 1). Methane was chosen to represent a non-sooty fuel and ethylene was chosen to represent a moderately sooty fuel. In these experiments, ignition was always initiated in 1-g just prior to the drop. The package was typically dropped within one second after ignition. The primary reason for not igniting in μg was the loss of time in heating the igniter wire and in stabilizing the flame after the initial ignition disturbances. Some photographs from these experiments are shown in the Color Plate 2.

The flame radius measured from such photographs along with the model predictions (to be discussed later) are shown in Fig. 2. As expected, for the same flow rates it was found that ethylene flames were much sootier and smaller. Immediately after dropping the package, the flame shape changed from a teardrop shape (see Color Plate 2) to a spherical shape (although it was not always completely spherical, probably because of slow large-scale air motion persisting inside the test chamber). The photographs shown in the Color Plate 2 are for medium flow rates of methane and low flow rates of ethylene. For the data presented in Fig. 2, an average flame radius determined from the photographs was used.

It is interesting to note that for both methane and ethylene (see the progressive flame growth in Color Plate 2), initially and in 1-g (e.g. photographs 'e' & 'f') the flame is nearly blue (non-sooty) but becomes bright yellow (sooty) immediately after the onset of μg conditions. Later, as the μg time progresses, the flame grows in size and becomes orange and less luminous and the soot seems to disappear. A possible explanation for this observed behavior is suggested by the theoretical calculations of Ref. 6. The soot volume fraction first quickly increases and later decreases as the local concentration of combustion products increases. Essentially, further soot formation is inhibited by the increase in the local concentration of the combustion products [Ref.7,8] and soot oxidation is enhanced. Thus, at the onset of μg conditions, initially a lot of soot is formed in the vicinity of the flame front (the outer faint blue envelope) resulting in bright yellow emission. As the flame grows, several events reduce the flame luminosity: (i) The soot is pushed toward cooler regions by thermophoresis. In fact, for sootier fuels this leads to the formation of a soot shell. (ii) The high concentration of combustion products left behind by the flame front inhibits soot formation and promotes soot oxidation.

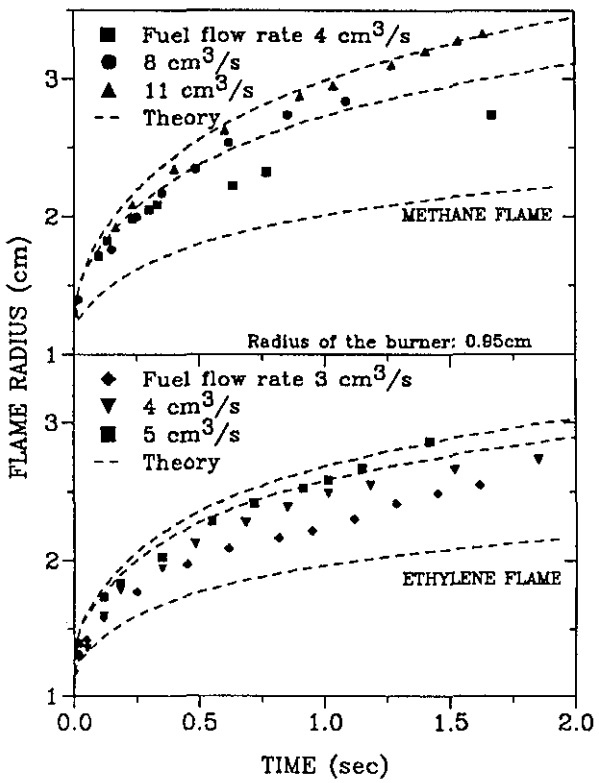

Figure 2: Flame radius versus time

(iii) The dilution and radiative heat losses caused by the increase in the concentration of combustion products reduces the flame temperature which in turn reduces the soot formation rate and the flame luminosity.

Figure 2 shows the average measured flame radius for methane and ethylene μg diffusion flames plotted against time. This is the radius of the outer faint blue region of the flame as measured from the photographs. To a good approximation this may be considered as the flame front location. Thus, as a first step, it will be interesting and important to determine if the transient expansion of the μg spherical diffusion flame can be theoretically predicted without considering soot formation and oxidation kinetics and flame radiation.

III. Model Formulation

As noted above, the spherical diffusion flames are expanding and changing their luminosity with time. Thus, the general theoretical formulation must be transient and must include flame radiation. For the simplest case of *constant pressure ideal gas reactions with Le=1*, we may write the following governing equations for any

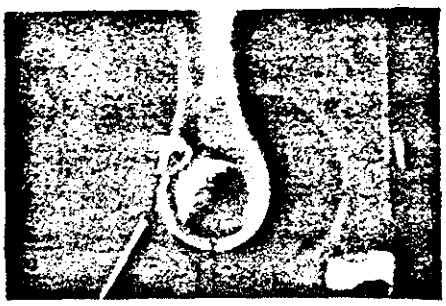

(a)

1-g flame

(b)

0.0667sec
into μg

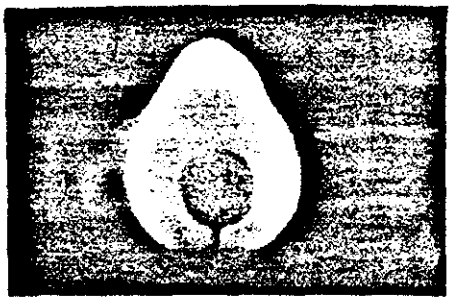

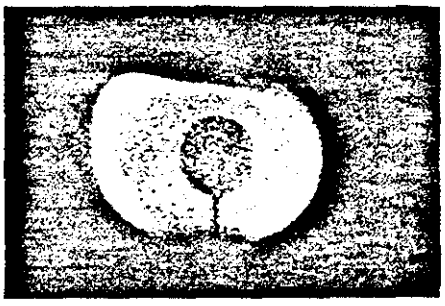

(c)

0.3333sec
into μg

(d)

0.6667sec
into μg

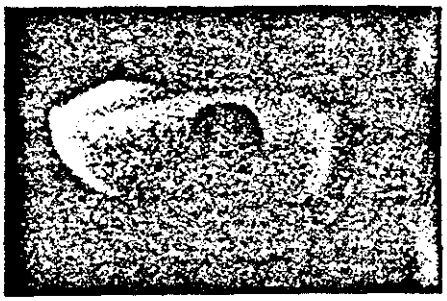

METHANE FLAME, FUEL FLOW RATE 8 cm^3/sec

(e)

1-g flame

(f)

0.0667sec
into μg

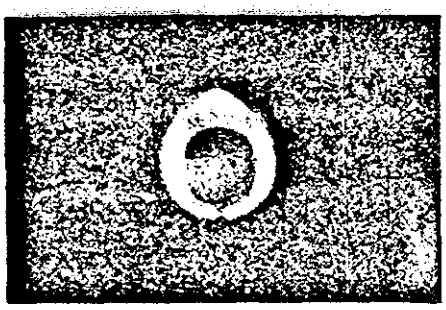

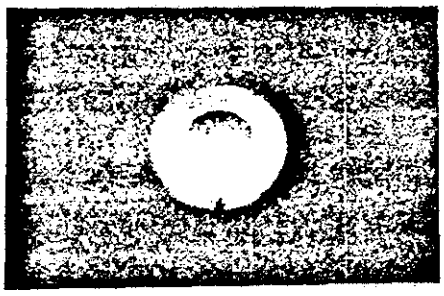

(g)

0.1667sec
into μg

(h)

0.5667sec
into μg

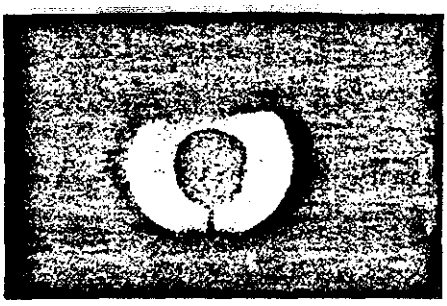

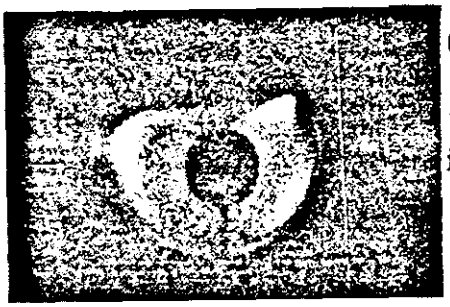

(i)

1.233sec
into μg

(j)

1.667sec
into μg

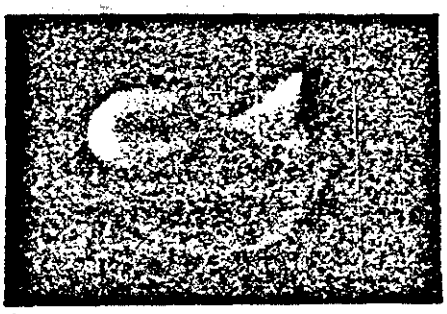

ETHYLENE FLAME, FUEL FLOW RATE 3 cm^3/sec COLOR PLATE 2

geometrical configuration (spherical or counterflow geometry):

Mass Conservation:

$$\frac{\partial \rho}{\partial t} + \nabla \cdot (\rho \vec{v}) = 0 \qquad (1)$$

Energy Conservation:

$$\rho \frac{\partial h^s}{\partial t} + \rho \vec{v} \cdot \nabla h^s - \nabla \cdot (\rho D \nabla h^s) = -\sum_i h_i^o W_i - Q_s \dot{m}_{S_o}''' - \nabla \cdot \vec{q}_r \qquad (2)$$

Constant Pressure Ideal Gas:

$$\rho T = \rho_\infty T_\infty \quad or \quad \rho h^s = const. \qquad (3)$$

Here, the symbols have their usual definitions with ρ = density, T = temperature, v = velocity, Y_i = mass fraction of species i, h^s = sensible enthalpy, w_i = mass production or destruction rate per unit volume of species i and D = diffusion coefficient. The last three terms in Equ (2) respectively are: the chemical heat release rate due to gas phase combustion, chemical heat released due to soot oxidation and the radiative heat loss rate per unit volume. The above equations, however, are insufficient for our problem because the soot volume fraction must be known as a function of space and time to determine the radiative heat loss. To enable describing soot volume fraction in a simple manner, we define the mass fraction of atomic constituents as follows: $\xi_j = \sum_i \left(M_j \nu_i^j / M_i\right) Y_i$, where M_i is the molecular weight of species i, M_j is the atomic weight of atom j and ν_i^j is the number of atoms of kind j in specie i. Assuming that the only atomic constituents present in the hydrocarbon flame are C, H, O & Inert and with $Y_{soot} \equiv \Phi \equiv \rho_s f_v / \rho$ (where: ρ_s= soot density & f_v = soot volume fraction), we obtain: $\xi_C + \xi_H + \xi_O + \xi_I + \rho_s f_v / \rho = 1$ Defining $\xi_C + \xi_H = \xi_F$ and $Z_F = \xi_F / Y_{F\infty}$ and $Z_o = \xi_o / Y_{o\infty}$, we obtain $Z = \left[(\xi_F)_{F\infty} Z_F + \rho_s f_v / \rho\right]$ as the conserved scalar for a sooty flame. This yields the following soot, fuel and oxidizer conservation equations in terms of their scalar variables:

Soot Conservation:

$$\rho \frac{\partial \Phi}{\partial t} + \rho \vec{v} \cdot \nabla(\Phi) - \nabla \cdot [\rho D_s \nabla(\Phi)] = \dot{m}_{S_p}''' - \dot{m}_{S_o}''' = \dot{m}_{net}''' \qquad (4)$$

Fuel Conservation:

$$\rho \frac{\partial Z_F}{\partial t} + \rho \vec{v} \cdot \nabla(Z_F) - \nabla \cdot [\rho D \nabla(Z_F)] = -\frac{1}{Y_{F\infty}} (\dot{m}_{S_p}''' - \dot{m}_{S_o}''') = -\frac{\dot{m}_{net}'''}{Y_{F\infty}} \qquad (5)$$

Oxygen Conservation:

$$\rho \frac{\partial Z_O}{\partial t} + \rho \vec{v} \cdot \nabla(Z_O) - \nabla \cdot [\rho D \nabla(Z_O)] = 0 \qquad (6)$$

Under conditions of small soot loading, the soot terms in the fuel and energy conservation equations can be ignored except when studying radiative extinction. Thus, Equ (5) may be considered homogeneous to a good approximation. Also, as a first crude approximation, the heat lost by flame radiation may be subtracted from the heat of combustion in the form of a radiative fraction. Thus, the energy equation (Equ(2)) can also be made homogeneous if written in terms of the total enthalpy [$h = \Sigma_i Y_i (h_i^\circ + h_i^s)$]. This approach may be adequate for calculating the observed expansion rate of the spherical diffusion flames, but it is completely inadequate for predicting radiative extinction. However, the great mathematical advantage of this approach is that it makes Eqs. (2, 4, 5, & 6) identical and only one conserved scalar equation need be considered. As a first step, it is of interest to see how well the transient expansion of the µg spherical diffusion flames be predicted without rigorously considering soot and gas radiation. This will also help in quantifying the effect of soot and gas radiation by comparison with more detailed calculations. Re-writing the above equations in spherical coordinates, we get:

Mass Conservation:

$$\frac{\partial \rho}{\partial t} + \frac{1}{r^2} \frac{\partial}{\partial r} (r^2 \rho v) = 0 \qquad (7)$$

Fuel Conservation:

$$\rho \frac{\partial Z}{\partial t} + \rho v \frac{\partial Z}{\partial r} - \frac{1}{r^2} \frac{\partial}{\partial r} \left(r^2 \rho D \frac{\partial Z}{\partial r} \right) = 0 \qquad (8)$$

These two equations along with the ideal gas law at constant pressure, Equ.(3), are sufficient to describe the

transient growth of non-radiative spherical diffusion flames and are expected to approximate this growth in the presence of flame radiation. It is also assumed that a fast one-step overall reaction occurs at the flame surface. This is represented by: $\nu_F F + \nu_O O \rightarrow \sum_{i=1}^{N-2} \nu_i P_i$ with q^o as the standard heat of reaction and $Q = q^o/M_F\nu_F$ the heat released per unit mass of fuel. Clearly,

$$q^o = h_F^o M_F \nu_F + h_O^o M_O \nu_O - \sum_{i=1}^{N-2} h_i^o M_i \nu_i .$$

The corresponding initial and boundary conditions for a sphere of radius 'R' blowing fuel gases at a rate $\dot{M}(t)$ are discussed below and illustrated in Figure 3.

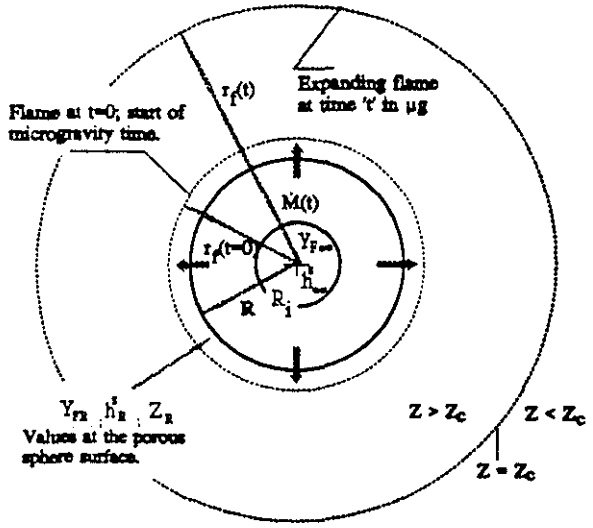

Figure 3: Schematic of the Model Problem

Continuity, fuel mass fraction and energy conservation at the surface of the sphere yield:

$$\frac{\dot{M}(t)}{4\pi R^2} = (\rho v)_{@R} \qquad (9a)$$

$$\frac{\dot{M}(t)}{4\pi R^2}\left(Y_{F\infty} - Y_{FR}\right) = -\rho D\left(\frac{\partial Y_F}{\partial r}\right)_{@R} \qquad (9b)$$

$$\frac{\dot{M}(t)}{4\pi R^2}\left(h^s_\infty - h^s_R\right) = -\rho D\left(\frac{\partial h^s}{\partial r}\right)_{@R} \qquad (9c)$$

Here, $Y_{F\infty}$ & h^s_∞ are the fuel mass fraction and enthalpy of the incoming fuel stream and Y_{FR} and h^s_R are the corresponding values at the outer surface of the sphere. The ambient values of fuel and oxidizer enthalpies are taken to be equal *i.e.* $h^s_\infty = h^s_{F\infty} = h^s_{O\infty}$ and $Z \equiv 1$ & $\rho \equiv \rho_o$ for ambient conditions on the fuel side and $Z \equiv 0$ & $\rho \equiv \rho_o$ for ambient conditions on the oxidizer side. Now, for high fuel injection rates, $Y_{F\infty} \approx Y_{FR}$; $h^s_\infty \approx h^s_R$ and $Z_R \approx 1$ and the corresponding diffusion terms in Equs. 9b & 9c become zero. For a given mass injection rate [$\dot{M}(t)$], these conditions are also satisfied as $R \rightarrow 0$. Thus, for a point fuel source, the boundary conditions at the source are simplified. Other initial and boundary conditions are: At t=0, Z(r,0); ρ(r,0) & v(r,0) are the spatial distributions corresponding to the flame at t=0, as shown in Figure 3. Also, at the flame surface [$r=r_f(t)$] $Z = Z_c = (1 + Y_{F\infty} M_O \nu_O / Y_{O\infty} M_F \nu_F)^{-1}$, and as $r \rightarrow \infty$, $Z \rightarrow 0$; $v \rightarrow 0$ & $h^s \rightarrow h^s_\infty$. All other variables can be easily obtained in terms of Z by utilizing the linear relationships between the conserved scalars [Ref.10]. For constant pressure ideal gas reactions these linear relationships yield:

For $R \le r < r_f(t)$:

$$\rho = \rho_o \left(1 + \frac{(1-z) Q Y_{F\infty} Z_c}{h^s_\infty (1 - Z_c)}\right)^{-1} \qquad (10)$$

$$v = \frac{\dot{M}(t)}{4\pi r^2 \rho_o} - \frac{D}{\rho}\frac{\partial \rho}{\partial r}$$

$$+ \frac{\dot{M}(t)}{4\pi r^2 \rho_o}\frac{Q Z_c}{h^s_\infty}\left(Y_{FR} - Y_{F\infty}\frac{(Z_R - Z_c)}{(1 - Z_c)}\right) \qquad (11)$$

These equations, along with Equ. (8), are sufficient to provide all the distributions in the region between the porous sphere and the flame. In Equ. (11), the first term on the right hand side represents the injection velocity and the second term accounts for the increase in the velocity due to the decrease in density. The third term is identically zero if the distribution of Y_F within the porous sphere (r<R) is identical to that in the gas i.e. $Y_F = Y_{F\infty}(Z - Z_c)/(1 - Z_c)$. Note at r=R, $Y_F = Y_{FR}$ and $Z = Z_R$. Also note that the third term becomes zero for high injection velocities and small 'R' since $Z_R \rightarrow 1$ & $Y_{FR} \rightarrow Y_{F\infty}$. In Equ. (11), ρ and $(\partial\rho / \partial r)$ can be expressed entirely in terms of Z through Equ. (10). Thus, Equ. (8) along with the appropriate boundary conditions is sufficient to determine Z(r,t).

At the flame surface $r=r_f(t)$:

At the flame surface, the $Z^{(-)} = Z^{(+)} = Z_c$ and all its derivatives are continuous. Here, '-' represents the fuel side and '+' represents the air side. Also, $T(r_f^+, t) = T(r_f^-, t) = T_f$; $\rho(r_f^+, t) = \rho(r_f^-, t) = \rho_f$ and $v(r_f^+, t) = v(r_f^-, t) = v_f$. Other jump conditions at the flame surface are obtained from species and energy balances as follows (assuming $Le = 1$ & $D = D_i$):

$$\left(\frac{\partial Y_F}{\partial r}\right)_{(r_f^-,t)} = -\left(\frac{M_F \nu_F}{M_O \nu_O}\right)\left(\frac{\partial Y_O}{\partial r}\right)_{(r_f^+,t)} \qquad (12)$$

$$\left(\frac{\partial h^s}{\partial r}\right)_{(r_f^-,t)} - \left(\frac{\partial h^s}{\partial r}\right)_{(r_f^+,t)} = -Q\left(\frac{\partial Y_F}{\partial r}\right)_{(r_f^-,t)} \qquad (13)$$

In terms of Z, both Equs. (12) & (13) are identically satisfied if the first derivatives of Z are equal at the flame surface. Thus, for the solution of Equ. (8) in the domain $r > r_f$, we only need to find expressions for ρ and v in terms of Z.

For $r_f(t) < r < \infty$:

$$\rho = \rho_o\left(1 + \frac{zQY_{F\infty}}{h^s_\infty}\right)^{-1} \qquad (14)$$

$$v = \frac{r_f^2(1-Z_c)}{r^2 Z_c}\left[\frac{v_f}{(1-Z_c)} - \frac{\dot{M}(t)}{4\pi r_f^2 \rho_o} - \frac{\dot{M}(t)QZ_c}{4\pi r_f^2 \rho_o h^s_\infty}\left(Y_{FR} - Y_{F\infty}\left(\frac{Z_R - Z_c}{1-Z_c}\right)\right)\right] - \frac{D}{\rho}\frac{\partial \rho}{\partial r} \qquad (15)$$

In the derivation of Equ. (15), gas velocity and density at the flame front are made continuous i.e. $v(r_f^+, t) = v(r_f^-, t) = v_f$. and $\rho(r_f^+, t) = \rho(r_f^-, t) = \rho_f$. Thus, v_f in Equ. (15) can be obtained from Equ. (11). Once again, the third term inside the bracket of Equ (15) becomes zero for reasons discussed above. Equs. (14), (15) and (8) along with the boundary conditions are sufficient to determine Z(r,t) for $r>r_f$.

IV Solution

Before discussing the solution procedure, let us examine the porous sphere used in the experiments. This sphere is quite small (19 mm dia.) and is constructed from a high porosity, low density and low heat capacity insulating material. Thus, its capacity to store heat and mass is negligible compared to the fuel injection rate which is injected inside the sphere (see Fig. 3). Hence, conditions inside the material of the sphere equilibrate on a time scale much shorter than the flame expansion time i.e. convection balances diffusion for any variable under consideration that can be described by an equation similar to Equ. (8). Neglecting radiation from the surface of the sphere, conservation conditions yield equations identical to Equs. 9(a) and 9(b) where ambient conditions are assumed to exist near the center of the sphere. Physically, the only purpose the porous sphere serves is to provide a radially uniform flow and it does not participate in energy and species balances because of its low storage capacity. Thus, the boundary conditions at the source can be applied at an arbitrarily small radius 'R' (chosen for numerical convenience) such that $Y_{F\infty} \approx Y_{FR}$; $h^s_\infty \approx h^s_R$ and $Z_R \approx 1$. This considerably simplifies Eqs. (11) & (15).

Equation (8), with Eqs. (10) & (11) for the fuel side and Eqs. (14) & (15) for the air side were numerically solved using the method of lines. A computer package entitled DSS2 was employed for this purpose. The calculated results for the flame location are shown plotted by dotted lines in Fig. 2. Property values used were those for air (ρ_o=1.16 10^{-3} gm/cm$_3$, D_o = 0.226 cm^2/s, T_∞ =298K, Cp =1.35 J/kgK) and the diffusion coefficient was assumed to vary as $T^{3/2}$ as predicted by kinetic theory of gases. Heat of combustion (Q) and mass based stoichiometric coefficient (v) used for methane and ethylene were Q=47465 J/gm and v=4 and Q=47465 J/gm and v=3.429 respectively. No assumptions other than those stated above were made to match the experimental data. Initial spatial distribution of Z(r,0) required for the flame at the start of μg time (i.e. at t=0) was taken as:

$$Z(r,0) = erfc\left(\frac{(r-R)erfc^{-1}(Z_c)}{(r_f - R)}\right) \qquad (16)$$

V Results and Discussion

Figure 2 shows the average radius of the outer faint blue regions for both methane and ethylene μg diffusion flames plotted against time. This radius was measured from the photographs. As stated above, the corresponding calculated results for the flame location are shown plotted with dotted lines. Given the approximations made in the model and the experimental errors, the comparison between the experimental and predicted flame radius is quite encouraging.

Numerical calculations also yield the instantaneous velocity and density profiles around the porous sphere during the flame expansion. These are shown plotted in Figures 4 & 5. Starting from the porous

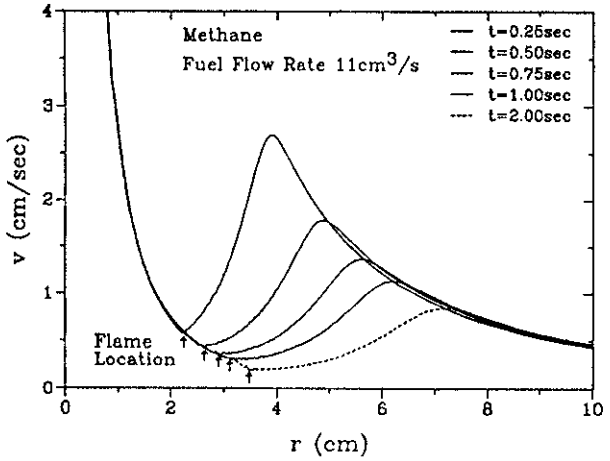

Figure 4: Radial velocity distribution at various instants

sphere (r=0.95), the gas velocity drops sharply and becomes a minimum at the flame location ($r=r_f$). Surprisingly, the mass flow rate at any location $r < r_f$ is found to be equal to the mass injection rate (i.e. $4\pi\rho v r^2 = \dot{M}(t)$). This implies that a similarity exists in the normalized coordinate $r/r_f(t)$ in the region $r < r_f(t)$. The density profiles in this region (Fig. 5) also show a similarity. Further reflection shows that this is to be

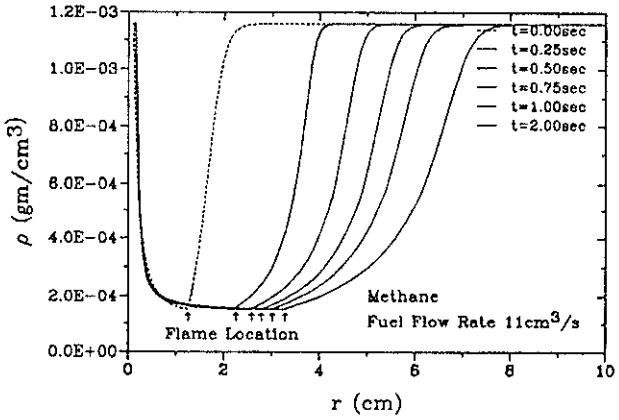

Figure 5: Radial density distribution at various instants

expected. In this problem, a constant temperature (adiabatic flame temperature) spherical flame is propagating outward starting from a small radius. In the spherical geometry, heat loss from the region surrounded by the flame is not possible. Thus, the only heat required by this region from the flame (in the absence of radiation) is to heat the injected mass $\dot{M}(t)$ to the flame temperature. Since, the injected mass is taken to be constant with time, a quasi steady state is developed. This is also observed in the density gradients at the flame on the fuel side (which are constant and are proportional to the temperature gradients). Applying a simple energy balance over the region $r \le r_f$, we obtain:

$$\frac{\dot{M}(t)}{4\pi r_f^2 \rho_f} = \frac{\dot{M}(t)}{4\pi r_f^2 \rho_o} - \frac{D}{\rho_f}\left(\frac{\partial \rho}{\partial r}\right)_f = v_f \quad (17)$$

Using Equ. (11) we find that at the flame $v_f = \dot{M}(t)/4\pi\rho_f r_f^2$. It is important to note that this is possible only because the injection rate is not varying with time.

VI Conclusions

In this work, experimental and theoretical results for expanding methane and ethylene diffusion flames in microgravity are presented. A small porous sphere made from a low-density and low-heat-capacity insulating material was used to uniformly supply fuel at a constant rate to the expanding diffusion flame. A theoretical model which includes soot and gas radiation is formulated but only the problem pertaining to the transient expansion of the flame is solved by assuming constant pressure infinitely fast one-step ideal gas reaction and unity Lewis number. This is a first step toward quantifying the effect of soot and gas radiation on these flames. The theoretically calculated expansion rate is in good agreement with the experimental results. Both experimental and theoretical results show that as the flame radius increases, the flame expansion process becomes diffusion controlled and the flame radius grows as $\sqrt{t}$. Theoretical calculations also show that for a constant fuel mass injection rate a quasi-steady state is developed in the region surrounded by the flame and the mass flow rate at any location inside this region equals the mass injection rate.

Acknowledgements: We would like to thank Mark Guether and Michael Johnston for their work on the Drop Tower apparatus. This project is supported at the University of Michigan by NASA grant NAG3-1460.

References

1.*Jackson, G., S., Avedisian, C., T. and Yang, J., C.*, Int. J. Heat Mass Transfer., Vol.35, No. 8, pp. 2017-2033, 1992.

2.*T'ien, J. S., Sacksteder, K. R., Ferkul, P. V. and Grayson, G. D.* "Combustion of Solid Fuels in very Low Speed Oxygen Streams," Second International Microgravity Combustion Workshop," NASA CP-10113, 1992.

3.*Ferkul, P., V.*, "A Model of Concurrent Flow Flame Spread Over a Thin Solid Fuel," NASA Contractor Report 191111, 1993.

4.*Ross, H. D., Sotos, R. G. and T'ien, J. S.*, Combustion Science and Technology, Vol. 75, pp. 155-160, 1991.

5.*T'ien, J. S.*, Combustion and Flame, Vol. 80, pp. 355-357, 1990.

6.*Atreya, A. and Agrawal, S.*, "Effect of Radiative Heat Loss on Diffusion Flames in Quiescent Microgravity Atmosphere," Accepted for publication in Combustion and Flame, 1993.

7.*Zhang, C., Atreya, A. and Lee, K.*, Twenty-Fourth (International) Symposium on Combustion, The Combustion Institute, pp. 1049-1057, 1992.

8.*Atreya, A. and Zhang, C.*, "A Global Model of Soot Formation derived from Experiments on Methane Counterflow Diffusion Flames," in preparation for submission to Combustion and Flame.

9.*Atreya, A.*, "Formation and Oxidation of Soot in Diffusion Flames," Annual Technical Report, GRI-91/0196, Gas Research Institute, November, 1991.

10.*Williams, F. A.*, "Combustion Theory," The Benjamin/Cummings Publishing Company, pp 73-76, 1985.